Title

Cryo-EM reveals different coronin binding modes for ADP— and ADP—BeFx actin filaments

Permalink

https://escholarship.org/uc/item/5bf3w5kq

Authors

Ge, Peng
Durer, Zeynep A Oztug
Kudryashov, Dmitri
et al.

Supplemental Material

https://escholarship.org/uc/item/5bf3w5kq#supplemental

Peer reviewed

Cryo-EM reveals different coronin binding modes for ADP– and ADP–BeFx actin filaments

Peng Ge[1,2,6], Zeynep A Oztug Durer[3,6], Dmitri Kudryashov[4], Z Hong Zhou[1,2,5] & Emil Reisler[3,5]

Essential cellular processes involving the actin cytoskeleton are regulated by auxiliary proteins that can sense the nucleotide state of actin. Here we report cryo-EM structures for ADP-bound and ADP–beryllium fluoride (ADP–BeFx, an ADP-P$_i$ mimic)-bound actin filaments in complex with the β-propeller domain of yeast coronin 1 (crn1), at 8.6-Å resolution. Our structures reveal the main differences in the interaction of coronin with the two nucleotide states of F-actin. We derived pseudoatomic models by fitting the atomic structures of actin and coronin into the EM envelopes and confirmed the identified interfaces on actin by chemical cross-linking, fluorescence spectroscopy and actin mutagenesis. The models offer a structural explanation for the nucleotide-dependent effects of coronin on cofilin-assisted remodeling of F-actin.

Dynamic remodeling of the actin cytoskeleton by actin-binding proteins (ABPs) is critical to many biological processes, including endocytosis, cell motility and cell division. This remodeling is linked to actin-filament age via a nucleotide-related clock. Actin filaments are distinctively different in their ATP- and ADP-bound states. ADP-bound, 'older' filaments (in which inorganic phosphate (P$_i$) has been released after ATP hydrolysis) were previously reported to be less stable[1] and to have more internal flexibility[2,3] relative to ATP and ADP-P$_i$ filaments. In particular, the lower-stability ADP–actin filaments have a higher dissociation rate constant at the barbed ends than either ATP–actin or ADP-P$_i$–actin filaments and lower association rate constants at both ends than ATP–actin filaments[4]. Biochemical evidence has suggested that structural changes in subdomain 2 of ADP–F-actin are correlated with its lower stability[5,6].

Cellular remodeling of actin structures includes, among other processes, filament severing, depolymerization and polymerization. The ADF and cofilin protein family is the main factor involved in actin filament severing[7,8], and members exhibit a strong preference for older filament segments (i.e., those in the ADP state). Cofilin severs F-actin more efficiently at subsaturating concentrations[8] at the boundaries between bare and decorated filament regions[9]. The Arp2/3 complex, a frequent partner of ADF and cofilin in the rapid reorganization of actin structures at the edge of the cell, stimulates new actin polymerization in branches radiating from the sides of existing filaments. The branch segments appear to be more stable in the ATP or ADP-Pi states of filaments[10,11]. However, despite functionally important differences in the affinities of some ABPs for the ATP, ADP-P$_i$ and ADP states of actin, such binding differences have not yet been examined by detailed structural analysis.

Nucleotide states of F-actin affect the binding of ABPs, which in turn regulate the function of ADF and cofilin and/or the Arp2/3 complex. The coronin family of proteins is a prime example of such cellular complexity. Coronins are broadly expressed in eukaryotic organisms[12,13] and can bind the Arp2/3 complex to affect branching of newly formed filaments[14–16]. They can also accelerate the severing of ADP–F-actin (but not ATP–F-actin) by cofilin[17]. Thus, coronins are considered to be important indirect regulators of actin dynamics in cell motility, endocytosis and phagocytosis[12]. Their malfunction in mice and humans is linked to immunodeficiency diseases[18–20].

Among the seven mammalian coronins, coronins 1–6 are highly homologous. They contain a well-conserved N-terminal segment followed by WD repeats arranged into a seven-bladed β-propeller structure, a unique region and the C-terminal coiled-coil (CC) domain[21,22]. Most previous functional studies have been done with type 1 coronins (1A, 1B and 1C), which include the yeast coronin, Crn1p. Both mammalian coronin 1B[14] and yeast Crn1p[23] have higher affinity toward ATP–F-actin than toward ADP–F-actin. In yeast, Crn1p has been reported to have a genetic and functional interaction with cofilin[17,23]. As described above, coronin inhibits cofilin-mediated severing of ATP–actin but promotes the severing of ADP–F-actin by cofilin[17].

As a first step toward understanding the molecular mechanism of coronin-cofilin effects on ATP–actin and ADP–actin filaments, we set out to obtain a structural description of the cofilin-actin and coronin-actin systems. A high-resolution (9 Å) cryo-EM structure of the cofilin–actin complex was recently reported[24]. Here, we applied helical reconstruction of cryo-EM images to solve two structures: coronin-decorated ADP–F-actin and ADP–BeFx–F-actin (a structural analog of ADP-Pi–F-actin). We observed two different modes of interaction between coronin and F-actin depending on actin's nucleotide state.

We obtained pseudoatomic models of F-actin–coronin complexes by docking atomic models of individual subunits into these two structures. These models led us to predict the interactions of the two proteins at residue-level detail. We provided independent experimental validation of these findings, using structure-based mutagenesis, chemical cross-linking methods and fluorescence measurements. Our results provide structural evidence for differential recognition of F-actin nucleotide states by one of F-actin's cellular binding partners. Furthermore, they suggest a mechanism for coronin's regulatory effects on remodeling of F-actin by cofilin and/or the Arp2/3 complex.

RESULTS

Coronin-bound ADP–F-actin and ADP–BeFx–F-actin structures

We observed in cryo-EM images that full-length Crn1p generated arrays of actin filaments (**Supplementary Fig. 1**), which were too dense for analysis by single-particle reconstruction methods. Consequently, we used a coronin construct (Crn1ΔCC; residues 1–600) lacking the CC domain, which is responsible for coronin oligomerization and actin bundling[23]. Class-average images of filament segments of these two complexes decorated with either full-length coronin or Crn1ΔCC were indistinguishable by two-dimensional classification-averaging analysis. Crn1ΔCC was also shown previously to function similarly to the full-length protein and to synergize with cofilin both in the *in vitro* and *in vivo* assays[25]. Therefore, we chose to pursue our structural analysis of coronin-bound F-actin by using Crn1ΔCC.

Crn1ΔCC extensively decorated both ADP-bound and ADP–BeFx–bound F-actin (**Fig. 1** and **Supplementary Fig. 2**) at a coronin/actin molar ratio of 3:1 to 4:1 (with actin set at 2 μM). At higher molar ratios, the background density of unbound coronin was limiting for structural analysis. In our images, the electron densities of coronin had a lower intensity than those of actin subunits, thus indicating that the decoration occupancy was probably less than 1:1 (coronin/actin). Alternatively, this lower density could result from the variable twist of F-actin, which has a stronger blurring effect at higher radius densities.

The resolutions of coronin-decorated ADP–F-actin and ADP–BeFx–F-actin structures are both 8.6 Å, as determined by the 'gold standard' 0.143 Fourier shell correlation criteria. At this resolution, every α-helix and some β-sheets of the actin subunits could be identified in the map (**Fig. 1**), and every β-sheet from the seven-bladed β-propeller of coronin could be visualized. Overall, actin subunits

from both the ADP and ADP–BeFx states closely resemble the previously determined F-actin structures[26,27]. The two actin nucleotide states have helical symmetries of 165.9° and 166.3° per subunit for ADP–F-actin and ADP–BeFx–F-actin, respectively (as reported from the customized Relion program, Online Methods). Actin subunits are similar in both states, with nearly all secondary-structure elements superimposable (**Fig. 1d,h**).

### Coronin footprint on ADP–F-actin and ADP–BeFx–F-actin

We obtained pseudoatomic models for the two nucleotide states of the actin–coronin complex by fitting the atomic model of F-actin[26] (per subunit) and the yeast homology model of the mouse coronin crystal structure[21] into our cryo-EM density maps. Both models could be unambiguously docked into their corresponding densities in both states (**Fig. 1c,d,g,h**). (For the pseudosymmetry of coronin, only one out of seven possible dockings was significantly favored, as indicated by the docking scores (**Supplementary Fig. 3**).) Coronin-actin interaction sites identified by this docking agree with the binding effects of actin mutagenesis reported below. They are also consistent with the loss of actin affinity of the coronin mutants[25] Crn1-2 (K10A R12A), Crn1-6 (R141A K142A), Crn1-13 (K295A D297A), Crn1-17 (E320A R323A) and Crn1-19 (R361A R362A E364A E365A). These indicated coronin residues and the critical actin residues identified by our mutagenesis experiments (below) are located at the coronin-actin interface suggested by our pseudoatomic models, thus validating these models.

In models for both nucleotide states, the common contacts of coronin were to subdomains 1 and 2 of 'i' actin and to subdomain 1 of '$i + 2$' actin, i.e., the consecutive subunit along the same filament strand (**Figs. 2** and **3** and **Supplementary Video 1**; details discussed below). However, the interaction of coronin with the opposite strand of the filament differed notably between the two states. In ADP–F-actin, we observed that coronin straddled the two filament strands by making extensive contacts to the opposite strand (through subdomains 3 and 4 of its '$i + 1$' actin and subdomain 4 of its '$i − 1$' actin) (**Fig. 2a**). This interaction may involve charge complementarity between $i + 1$ actin's residues Asp222, Lys315 and Glu316 and their respective pairs on coronin, Lys20, Glu22 and Lys21 (**Fig. 2a**). In contrast, coronin contacts to the other strand are weak in the ADP–BeFx state[28,29] (mimicking the ADP-P$_i$ state of the filament[30]) and involve subdomain 4 of the $i + 1$ actin only slightly (**Fig. 2b**). One likely charge interaction in this state could be between Lys21 and Lys69 of coronin and Glu224 on subdomain 4 of $i + 1$ actin. These residues are close together and could interact by charge complementarity when in favorable rotamers (**Fig. 2b**).

The difference between the two binding modes of coronin can be explained as a rotation by approximately 20° around an axis passing through residues Asp183, Arg202 and Lys227 of coronin (**Fig. 2a** and **Supplementary Video 1**). As a result of this rotation, the interface of coronin with subdomain 1 of actin subunit i in both ADP and ADP-P$_i$ states was largely preserved. However, distant contacts with actin
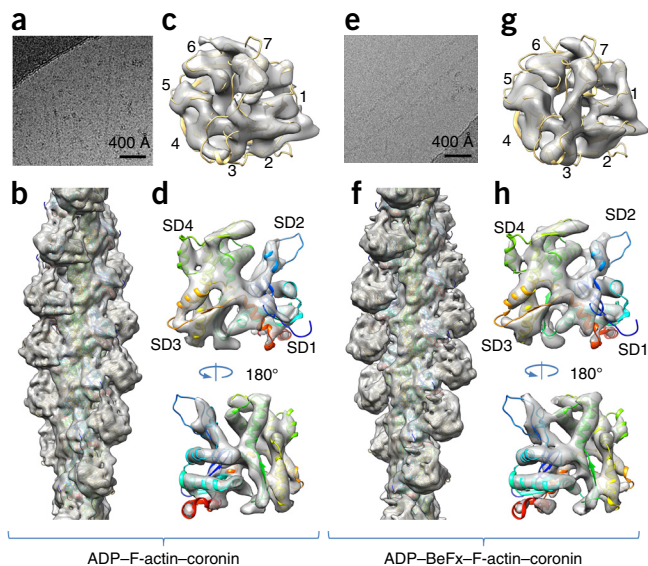
Figure 1 Cryo-EM reconstruction of coronin-decorated actin filaments in both ADP and ADP–BeFx states. (**a**–**d**) ADP state. (**e**–**h**) ADP–BeFx state. (**a**,**e**) Areas of original images. (**b**,**f**) Cryo-EM reconstruction of coronin (Crn1ΔCC)-decorated actin filaments (gray envelope) with an atomic model of actin and our homology model of coronin fitted (in ribbons: actin, rainbow colors; coronin, gold; described in main text). (**c**,**g**) Densities corresponding to coronin (gray envelope) alone fitted with its atomic model (ribbon). The indexes of the blades of the propeller are labeled 1–7. (**d**,**h**) Densities corresponding to actin (gray envelope) alone fitted with its atomic model (ribbon). SD, subdomain.
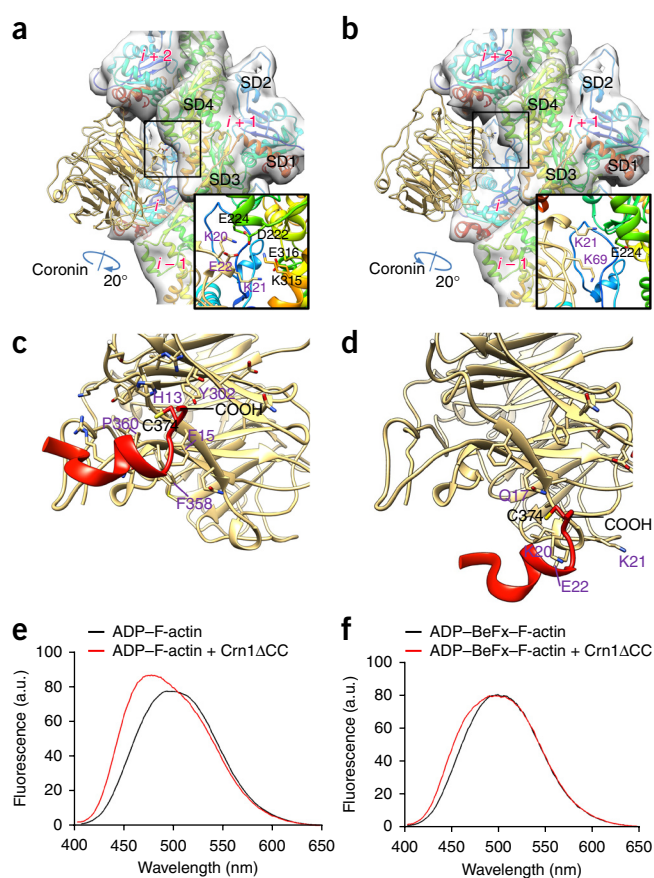
Figure 2 Different interaction modes between coronin and actin in ADP and ADP–BeFx states. (**a–d**) Pseudoatomic models obtained by fitting an atomic model of actin and our homology model of coronin into our cryo-EM densities (described in main text). (**a,b**) Differences in the overall binding modes between coronin and actin in ADP (**a**) and ADP–BeFx (**b**) states. Actin is shown in rainbow-colored ribbons (blue, N terminal; red, C terminal), with each subunit delineated with its gray transparent surface derived from its atomic model; coronin is shown in gold ribbons. Key interacting amino acids between coronin and actin $i + 1$ are shown in sticks and are highlighted in insets. (**c,d**) Different environments of Cys374 in ADP (**c**) and ADP–BeFx (**d**) states. Actin's C-terminal loop 371–375 is in red; the C terminus is marked by COOH. (**e,f**) Fluorescence emission spectra (in arbitrary units, a.u.) of actin labeled with acrylodan at residue 374 in the ADP–actin–coronin complex (**e**) and the ADP–BeFx–actin–coronin complex (**f**). In **a–d**, key residues are marked in black and purple for actin and coronin, respectively.

$i + 2$ (**Fig. 2**). In our model of the ADP state, the C-terminal loop of actin (residues 371–375) faces a hydrophobic environment on coronin composed of His13, Phe15, Phe358 and Pro360 (**Fig. 2c**). In contrast, our model of the ADP–BeFx state shows that the same actin loop faces a polar environment on coronin, composed of residues 17–22 (Gln17, Lys20, Lys21 and Glu22) (**Fig. 2d**). To test this, we attached a small fluorescent probe, acrylodan, to actin's C-terminal Cys374. In agreement with our models, coronin binding caused a larger blueshift in the spectrum of acrylodan-labeled ADP–F-actin than acrylodan-labeled ADP–BeFx-actin (**Fig. 2e,f**), thus supporting its greater burial in a hydrophobic environment in the ADP–F-actin. Notably, binding of several other ABPs to actin has also been shown to be modulated by conformational changes in actin's C-terminal region[31–33].

Ionic interactions govern coronin binding to F-actin
Pseudoatomic models of the actin–coronin complexes suggest that major interactions between coronin and F-actin are predominantly electrostatic and similar in both nucleotide states. Indeed, an increase in the buffer ionic strength (from 50 mM to 150 mM KCl) decreased

subunit $i + 2$ and, in particular, contacts with the opposite strand were affected substantially (**Supplementary Video 1**).

Another difference between the two nucleotide-state structures appears in the interaction of coronin with subdomain 1 of actin subunit

Figure 3 Interactions between coronin and filamentous actin in the ADP state. (**a–d**) Pseudoatomic models obtained by fitting an atomic model of actin and our homology model of coronin into cryo-EM densities (described in main text). (**a**) Overview of actin-coronin interaction. One coronin subunit (red, white and blue surface) and its four neighboring actin subunits (gray surfaces with rainbow-colored ribbons) are shown from front and back. SD, subdomain; i, the actin subunit that most intensively interacts with this coronin subunit. $i + 1$, $i + 2$ and $i - 1$ mark the relative positions of adjacent actin subunits in the filament. Key interactions are boxed and are highlighted in connected panels. In all panels, actin subunits are delineated by gray transparent surfaces derived from their atomic models. (**b**) Interaction between the D loop of actin and coronin. Residues Arg37 and Lys50 face a negatively charged patch on coronin. (**c**) Interaction between actin's C-terminal (COOH) helices (red ribbons in actin model) and coronin. Left, interaction between coronin and actin $i + 2$; right, interaction between coronin and actin i. (**d**) The most critical charge interactions between coronin and actin. These

are concentrated on actin's helix 79–93 (asterisk in **a** and **d**) with extension to amino acid 100. (For clarity, residues 78–100 are shown exclusively in cyan ribbon, with key amino acids shown as sticks.) Throughout figure, key residues are colored in black and purple for actin and coronin, respectively.
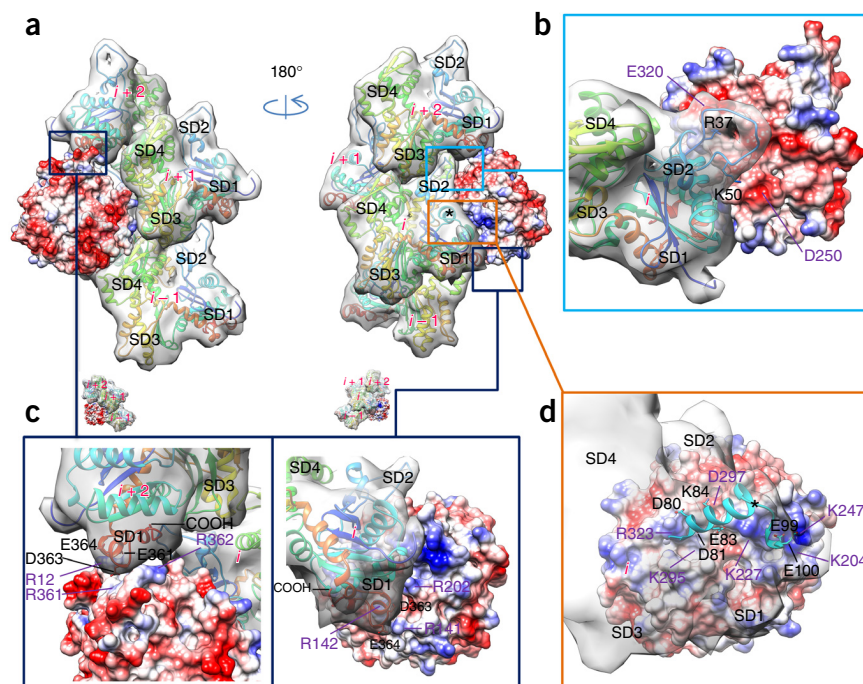
Figure 4 Charge and shape complementarity between actin and coronin. Pseudoatomic models obtained by fitting an atomic model of actin and our homology model of coronin into our cryo-EM densities (described in main text). Top, the pseudoatomic model of the actin–coronin complex, shown in molecular surface colored by surface charge. The surface for coronin (right) is semitransparent, showing the ribbon model of coronin. Bottom, the interface between actin and coronin is shown in open-book configuration with each interacting surface turned 90° toward the page. The charged interactions between the two are concentrated in a triangle (blue).

Actin   Coronin
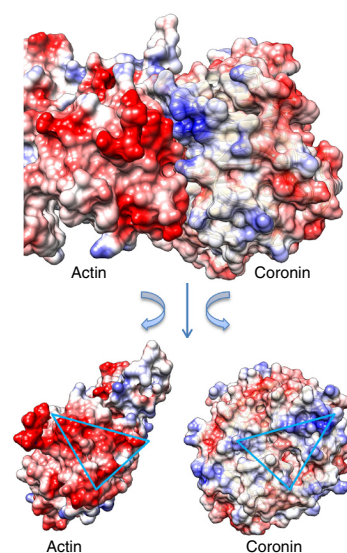
Actin   Coronin

coronin-actin binding affinity by two-fold (**Table 1**). The proposed interface between coronin and actin shows good charge and shape complementarity. Actin *i*, which has the greatest contact area with coronin (**Fig. 3a**), has extensive electrostatic interactions with a prominent positively charged 'corridor' on the 'top' surface of the coronin's β-propeller domain (**Fig. 4**). The charged corridor on coronin is composed of Lys204, Lys227 and Lys247 and Arg323. These three lysines interact synergistically and respectively with Glu99, Glu83 and Glu100 on actin *i* (**Fig. 3d**). In our model, Arg323 is in proximity (4–6 Å) to actin's Asp80-Asp81 acidic patch. These putative ionic interactions with coronin span the entire actin helix 78–92, with an extension to Glu100. Because this charged corridor largely coincides with the rotation axis (described above), its interactions with both ADP and ADP–BeFx actins are mainly preserved (**Supplementary Video 1**).

Another important charge-interaction region at the actin and coronin interface in our model involves a cluster of actin residues (Glu361, Asp363 and Glu364) and coronin arginines (Arg361 and Arg362) (**Fig. 3c**). Actin's Asp363 and Glu364 make contacts with two consecutive coronins along the same actin filament strand (or, conversely, two different regions of the same coronin molecule contact the Asp363-Glu364 patch on two consecutive actin monomers in the same long-pitch strand (**Fig. 3c**)). Specifically, Asp363 and Glu364 of *i* actin are in proximity to coronin's Arg141 and Lys142. Residues Glu361, Asp363 and Glu364 on the neighboring (*i* + 2) actin are positioned close to the same coronin's Arg361 and Arg362. This arrangement occurs in both nucleotide states of actin, albeit with different charge-charge interactions being coupled in each case, as described above (**Fig. 3c**).

Other noticeable interactions between coronin and actin in our model include Lys50 (on *i* actin's D loop), which interacts with a patch of negative charges on coronin around Asp273 (**Fig. 3b**). In addition, *i* actin's Lys37 faces another patch of negative charges on coronin concentrated around Glu320 (**Fig. 3b**). The two patches are positioned similarly in both nucleotide-state models; however, the intrinsic flexibility of the D loop, the presence of oppositely charged Asp51 and the insufficient resolution of our structures make it difficult to accurately compare these regions in the two nucleotide states. Importantly, the C terminus and the D loop of actin are well-recognized nucleotide-state sensors of actin (reviewed in ref. 34). We therefore speculate that the differences in coronin binding to ADP and ADP–BeFx actin originate from nucleotide-dependent conformational transitions in these areas.

We verified the importance of the interactions reported above via mutagenesis of actin and by determining the binding affinity of mutant ADP-bound actins for coronin (**Table 1** and **Supplementary Figs. 4** and **5**). On the basis of our pseudoatomic model of the coronin–actin complex, the lysine patch 204–207 on coronin has a crucial role in actin binding. Indeed, mutating complementary residues on actin (Glu99 and Glu100) to alanines caused the binding affinity of coronin for F-actin to decrease 18-fold compared to that for wild-type actin. Glu83-Asp84 and Asp363-Glu364 of actin are also critical for coronin's binding. Their substitution with alanines decreases the

binding affinity of these mutants seven- and five-fold, respectively. Interestingly, Asp363-Glu364 are located at the border between two consecutively bound coronin molecules, thus making it possible for this negative patch on actin to contribute to the binding of both coronins. Moreover, the sensitivity of actin's C terminus to the nucleotide state argues for its role in the observed nucleotide-dependent interaction patterns of coronin and actin. In line with the results of the above actin mutations, mutants of complementary residues on coronin identified in this study (Arg141-Lys142 in one positive patch and Arg361-Arg362 in another) were previously shown to severely affect coronin's binding to F-actin[25]. Other mapped interactions of coronin with actin contribute less to their binding energy, thus resulting in up to a two-fold affinity decrease when the respective actin residues are mutated to alanine (**Table 1**).

In another approach to test actin's charge interactions with coronin, we carried out zero-length chemical cross-linking with 1-ethyl-3-(3-dimethylaminopropyl) carbodiimide (EDC)[35–37]. EDC

Table 1 Summary of Crn1-ΔCC binding affinities for wild-type and mutant yeast actins

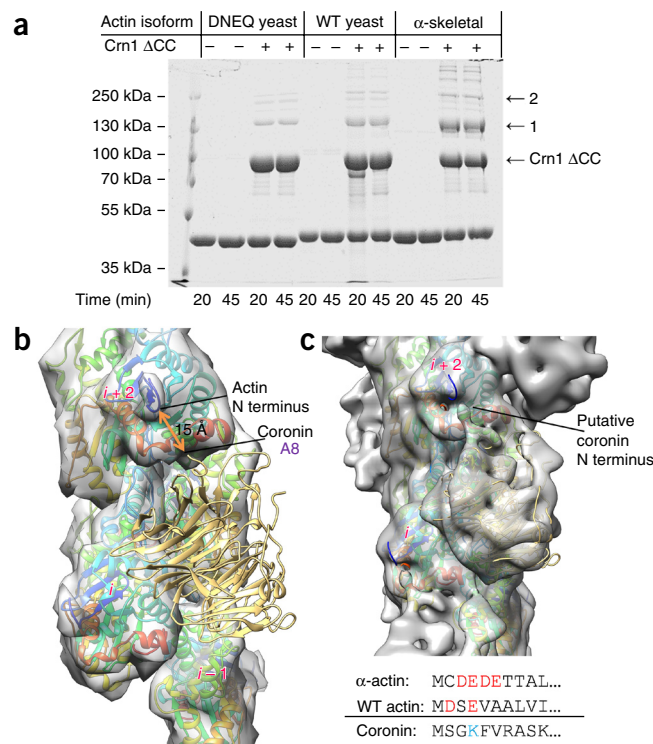|	K_d (μM)	$K_d/K_{d\ WT}$	Coronin residues in proximity
WT	0.87 ± 0.04	1.00	
DNEQ[a]	0.81 ± 0.01	~1	
ΔDSE[b]	0.76 ± 0.03	~1	
K50A D51A (red)[c]	1.55 ± 0.06	~2	D250 and D273
D80A D81A (magenta)	1.9 ± 0.5	~2	R323 and K295
E83A K84A (blue)	5.8 ± 0.3	~7	K227 and D297
E99A E100A (cyan)	16	~18	K204 and K247
K315A E316A (green)	1.4 ± 0.1	~1.6	K20, K21 and E22 (with actin *i* + 1)
D363A E364A (yellow)	4.4 ± 0.8	~5	R141, R142 and R202 (with actin *i*)
			R361 and R362 (with actin *i* + 2)
R37A R39A (orange) + phalloidin[d]	2.7 ± 0.1	~3	E320
WT + 150 mM KCl	2.3	~2–3	

[a]D2N E4Q, actin mutant with a neutralized N terminus. [b]ΔDSE, mutant actin with its three N-terminal residues deleted. [c]Color names in parentheses refer to the colors of these residues in **Supplementary Figure 5**. [d]This set of measurement was carried out in the presence of equimolar concentrations of phalloidin. WT, wild type.

Figure 5 Crn1ΔCC and ADP–F-actin are cross-linked by EDC mainly, but not only, through actin's N terminus. (**a**) SDS-PAGE analysis of actin-coronin EDC cross-linking. EDC-activated α-skeletal, wild-type yeast (WT) and DNEQ F-actins were cross-linked with equimolar amounts of Crn1ΔCC for 20 or 45 min as indicated and then analyzed by SDS-PAGE. '1' indicates one actin in a complex with one coronin molecule; '2' indicates a protein complex involving more than one actin per coronin molecule. (**b**) Side view of the pseudoatomic model of the actin–coronin complex, showing proximity of the N termini of actin (ribbons in rainbow colors with gray transparent surfaces derived from the atomic model) and coronin (gold ribbons). The orange arrow points to actin residue 1 and coronin residue 8. (**c**) Patch of density attributed to the N-terminal residues of coronin extends from coronin toward the N terminus of actin. N-terminal amino acid sequences are given for α-skeletal actin, wild-type yeast actin and coronin. Charged residues that are likely to be involved in EDC cross-linking are highlighted in blue and red.

can be used to activate acidic residues on actin, mainly at its N terminus, and then to covalently link them to amine groups in the bound protein[35–37]. We observed that EDC-activated skeletal α-actin filaments could be covalently cross-linked to coronin (**Fig. 5a**). The cross-linking may occur to the N terminus of coronin. This is suggested by the proximity of actin's N terminus in the cryo-EM map (**Fig. 5b**) to the extra density that can be ascribed to the N-terminal residues of coronin (**Fig. 5c**). Interestingly, yeast coronin cross-linked less efficiently to yeast actin than to rabbit skeletal α-actin (**Fig. 5a**). This was most probably because yeast actin's N terminus contains only two negatively charged residues, whereas α-actin's N terminus contains four (**Fig. 5**). Indeed, when we used a yeast actin mutant with a neutralized N terminus, D2N E4Q (DNEQ actin)[38], its EDC-activated cross-linking to coronin was the lowest (**Fig. 5a**). A minor amount of cross-linked actin–coronin complex formed with that actin mutant (**Fig. 5a**) could arise from EDC activation of actin residues Glu99-Glu100 (ref. 39) and Asp363-Glu364 (refs. 36,37). Interestingly, DNEQ actin and yeast actin with its three N-terminal residues deleted (ΔDSE[38]) showed less than 50% change in their binding affinity for coronin relative to wild-type actin (**Table 1**), thus indicating a low overall contribution of actin's N terminus to coronin binding.
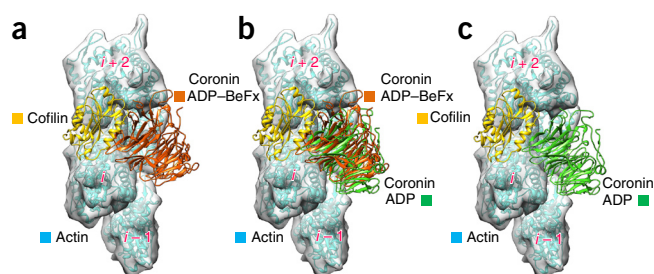
DISCUSSION

Our structural analysis of coronin–actin complexes stems from our interest in deciphering coronin's roles in assisting Arp2/3

Figure 6 Modeling of cofilin on the coronin-decorated F-actin in ADP–BeFx and ADP states. (**a**) The pseudoatomic models of actin–coronin in the ADP–BeFx state and actin–cofilin are superimposed by alignment of actin *i*. For clarity, actin subunits are shown for the actin–coronin complex in the ADP state only and are delineated by gray transparent surfaces derived from the atomic model. (**b**) For comparison, the pseudoatomic model of actin–coronin in the ADP state is superimposed on the previous model in a similar way. (**c**) A separate model that includes only actin–coronin in the ADP state and cofilin superimposed as in **a**. A noticeable main chain clash between coronin and cofilin can be seen in the ADP–BeFx state (**a**) but not in the ADP state (**c**).

complex–mediated actin branching and in regulating the nucleotide-dependent severing of actin filaments by cofilin (reviewed in refs. 12,13). The initial step toward understanding the mechanism of such complex interactions and effects of coronin is to obtain a structural map of its complex with actin filaments in both the ADP and ADP-P$_i$ (ADP–BeFx in this study) states.

Low-resolution negative-stain EM analysis of coronin–F-actin led to specific predictions of contact surfaces between these proteins[40]. However, mutational scanning of clusters of charged residues on coronin and assays of their effect on the affinity for actin suggested a set of different actin-interaction sites on coronin[25]. The pseudoatomic models of coronin–F-actin structures (in ADP and ADP–BeFx states) derived from our cryo-EM data (**Fig. 1** and **Supplementary Fig. 2**) are consistent with the loss of affinity for actin in the coronin mutants[25] Crn1-2 (K10A R12A), Crn1-6 (R141A K142A), Crn1-13 (K295A D297A), Crn1-17 (E320A R323A) and Crn1-19 (R361A R362A E364A E365A). All of these clusters are located at the coronin-actin interface proposed in the present study (**Figs. 2** and **3**, **Supplementary Fig. 4** and **Supplementary Table 1**). Our ADP–actin–coronin model suggests that the coronin residues identified by Gandhi and co-workers[25] make contacts with actin residues 37, 39, 50, 51, 80–84 and 360–364 (**Supplementary Table 1** and **Figs. 2** and **3**). Indeed, our results (**Table 1** and **Supplementary Fig. 4**) showed that ADP–actin filaments of R37A R39A, K50A D51A, D80A D81A, E83A D84A and D363A E364A mutants had a decrease of at least two-fold in their binding affinity to coronin. The affinity decrease was greater when a mutation on actin affected several corresponding binding sites on Crn1-ΔCC, for example, D363A E364A (**Supplementary Table 1**). Notably, as predicted by our model of actin-coronin contacts, mutation of Glu99 and Glu100 had a large impact on coronin-actin binding (**Table 1**). The interest in this site is augmented by its contribution to the binding of several other ABPs such as myosin[41–43], drebrin[44], actobindin[45] and even a glycolytic enzyme, aldolase[46]. Conceivably, such interactivity of this site may be implicated in competitive compartmentalization of these, and perhaps other, F-actin–binding proteins in various regions

of the cell. Overall, both actin-based mutagenesis and cryo-EM–based models are in agreement with the actin binding footprint on coronin identified by Gandhi and co-workers[25]. Obviously, the actin–coronin structure reported here is at higher resolution and is more comprehensive than in previous models (**Fig. 1**).

Functional assays of coronin's effect on actin-filament severing by cofilin have indicated that coronin should not interfere with cofilin binding to ADP–actin, even though it may inhibit cofilin binding to ATP–actin[13,17]. Our work provides a structural explanation for the cooperation between cofilin and coronin. When we superimpose our models with Galkin *et al.*'s high-resolution cryo-EM model of F-actin and human cofilin 2 (ref. 24), there is a partial clash of coronin and cofilin binding maps (**Fig. 6a,b** and **Supplementary Video 2**) in the ADP-P$_i$ state (simulated by the ADP–BeFx complex in this study). This suggests their binding competition and offers an explanation for coronin's protection of freshly polymerized filaments (mainly in the ADP-P$_i$ state) from severing. Importantly, in the ADP state of F-actin the steric clash observed between blade 5 of coronin and the N-terminal helix of cofilin is released (**Fig. 6c**). Thus, as judged by the immediate proximity of the surfaces of coronin (this work) and cofilin[24] in the superimposed reconstructions (**Fig. 6c**), coronin would allow and/or promote cofilin binding to result in greater severing in the ADP state of F-actin[17,25]. Furthermore, because shearing of actin filaments by cofilin occurs mainly at the boundaries between cofilin-decorated and undecorated segments[47], it is plausible that coronin may support the formation of such boundaries by reinforcing the bare actin–like conformation at the sites that it occupies while also promoting adjacent binding of cofilin.

Next, to gain insight into the structural basis of concentration-dependent inhibition and activation of the Arp2/3 complex in the presence of coronin[12,16], we superimposed our actin–coronin models and the Arp2/3 complex–actin filament model[48]. The location of coronin on the mother filament overlaps with that of the Arp2/3 complex in both nucleotide models (**Supplementary Fig. 6**), because the footprints of coronin on actin *i* and *i* + 2 clash with ArpC3 and ArpC2–ArpC4, respectively. Therefore, at high levels of coronin decoration, binding of the Arp2/3 complex to F-actin would be inhibited, in agreement with previous structural findings[48]. However, under nonsaturating conditions coronin and Arp2/3 complex can bind next to each other and even promote mutual recruitment to actin filaments. This is consistent with the reported coronin concentration–dependent switch of the Arp2/3 complex's activity[12,16].

Nucleotide-based conformational rearrangements in both G- and F-actin are critical in modulating and controlling actin dynamics at the cellular level. Several areas on the actin subunit are recognized as primary and secondary conformational sensors. The primary sensors are located in direct proximity to the nucleotide-binding cleft and transfer conformational changes from the nucleotide to peripheral sensors (reviewed in ref. 34). The secondary sensors are peripherally located; they control nucleotide-dependent differential binding of regulatory proteins. Among the four well-recognized peripheral sensory regions—the V stretch (residues 227–237)[49], W loop (residues 165–172)[50], D loop (residues 40–51)[51,52] and C terminus[53]—the latter two make prominent contacts with coronin and are likely to contribute to the observed nucleotide-state differences. The D loop is not well defined in our reconstructions, and therefore its role in the observed transitions is speculative at this stage. However, the footprint of coronin binding to the C-terminal helix of actin (residues 350–364) clearly differs in the two nucleotide states, with more-prominent contacts detected in the ADP–BeFx state (**Fig. 2c,d**). Mutations on actin that involve this region (**Table 1**), as well as the corresponding mutations

on coronin[25], severely affect the affinity of these proteins for each other. Therefore, tighter binding of coronin to the C terminus of *i* + 2 actin in the ADP–BeFx state may override the larger contact area between coronin and the *i* + 1 actin subunit on the opposite strand of actin. The C terminus of actin, which participates in the binding of two consecutive coronin molecules, is known to be allosterically coupled[53] to the D loop, thereby adding indirect support for the role of these two areas in nucleotide-dependent regulation of coronin-actin interactions.

In conclusion, we provided intermediate-resolution cryo-EM images of the coronin–actin complex and predicted protein-protein contacts with high precision. We also presented specific nucleotide-state differences in the structure of actin–coronin complexes. To the best of our knowledge, this is the first report of structural mapping of nucleotide state–driven differences in actin–ABP complexes, and it includes the best-resolution structures of such complexes. When combined with the previously reported structures of actin–cofilin and actin–Arp2/3 complex, our model offers structural explanations for coronin's regulation of cofilin and the Arp2/3 complex's interactions with ADP–actin and ADP-P$_i$–actin.

METHODS

Methods and any associated references are available in the online version of the paper.

Accession codes. The cryo-EM maps of the ADP–F-actin–coronin and ADP–BeFx–F-actin–coronin complexes have been deposited in the Electron Microscopy Data Bank under accession codes EMD-6100 and EMD-6101, respectively.

Note: Any Supplementary Information and Source Data files are available in the online version of the paper.

AUTHOR CONTRIBUTIONS
P.G., Z.A.O.D., D.K. and E.R. designed experiments; P.G., Z.A.O.D. and D.K., collected EM data; P.G. and Z.H.Z. processed, analyzed and interpreted EM data; Z.A.O.D. collected and analyzed biochemical data; all authors wrote and reviewed the manuscript.

1. Orlova, A. & Egelman, E.H. Structural basis for the destabilization of F-actin by phosphate release following ATP hydrolysis. *J. Mol. Biol.* **227**, 1043–1053 (1992).
2. Isambert, H. *et al.* Flexibility of actin filaments derived from thermal fluctuations: effect of bound nucleotide, phalloidin, and muscle regulatory proteins. *J. Biol. Chem.* **270**, 11437–11444 (1995).
3. Orlova, A. & Egelman, E.H. A conformational change in the actin subunit can change the flexibility of the actin filament. *J. Mol. Biol.* **232**, 334–341 (1993).
4. Fujiwara, I., Vavylonis, D. & Pollard, T.D. Polymerization kinetics of ADP- and ADP-Pi-actin determined by fluorescence microscopy. *Proc. Natl. Acad. Sci. USA* **104**, 8827–8832 (2007).
5. Khaitlina, S.Y. & Strzelecka-Golaszewska, H. Role of the DNase-I-binding loop in dynamic properties of actin filament. *Biophys. J.* **82**, 321–334 (2002).

6. Muhlrad, A., Cheung, P., Phan, B.C., Miller, C. & Reisler, E. Dynamic properties of actin: structural changes induced by beryllium fluoride. *J. Biol. Chem.* **269**, 11852–11858 (1994).
7. Bamburg, J.R., McGough, A. & Ono, S. Putting a new twist on actin: ADF/cofilins modulate actin dynamics. *Trends Cell Biol.* **9**, 364–370 (1999).
8. Andrianantoandro, E. & Pollard, T.D. Mechanism of actin filament turnover by severing and nucleation at different concentrations of ADF/cofilin. *Mol. Cell* **24**, 13–23 (2006).
9. Suarez, C. *et al.* Cofilin tunes the nucleotide state of actin filaments and severs at bare and decorated segment boundaries. *Curr. Biol.* **21**, 862–868 (2011).
10. Blanchoin, L., Pollard, T.D. & Mullins, R.D. Interactions of ADF/cofilin, Arp2/3 complex, capping protein and profilin in remodeling of branched actin filament networks. *Curr. Biol.* **10**, 1273–1282 (2000).
11. Pollard, T.D. & Borisy, G.G. Cellular motility driven by assembly and disassembly of actin filaments. *Cell* **112**, 453–465 (2003).
12. Chan, K.T., Creed, S.J. & Bear, J.E. Unraveling the enigma: progress towards understanding the coronin family of actin regulators. *Trends Cell Biol.* **21**, 481–488 (2011).
13. Gandhi, M. & Goode, B.L. Coronin: the double-edged sword of actin dynamics. *Subcell. Biochem.* **48**, 72–87 (2008).
14. Cai, L., Makhov, A.M. & Bear, J.E. F-actin binding is essential for coronin 1B function *in vivo*. *J. Cell Sci.* **120**, 1779–1790 (2007).
15. Humphries, C.L. *et al.* Direct regulation of Arp2/3 complex activity and function by the actin binding protein coronin. *J. Cell Biol.* **159**, 993–1004 (2002).
16. Liu, S.L., Needham, K.M., May, J.R. & Nolen, B.J. Mechanism of a concentration-dependent switch between activation and inhibition of Arp2/3 complex by coronin. *J. Biol. Chem.* **286**, 17039–17046 (2011).
17. Gandhi, M., Achard, V., Blanchoin, L. & Goode, B.L. Coronin switches roles in actin disassembly depending on the nucleotide state of actin. *Mol. Cell* **34**, 364–374 (2009).
18. Mueller, P. *et al.* Regulation of T cell survival through coronin-1–mediated generation of inositol-1,4,5-trisphosphate and calcium mobilization after T cell receptor triggering. *Nat. Immunol.* **9**, 424–431 (2008).
19. Shiow, L.R. *et al.* Severe combined immunodeficiency (SCID) and attention deficit hyperactivity disorder (ADHD) associated with a Coronin-1A mutation and a chromosome 16p11.2 deletion. *Clin. Immunol.* **131**, 24–30 (2009).
20. Shiow, L.R. *et al.* The actin regulator coronin 1A is mutant in a thymic egress-deficient mouse strain and in a patient with severe combined immunodeficiency. *Nat. Immunol.* **9**, 1307–1315 (2008).
21. Appleton, B.A., Wu, P. & Wiesmann, C. The crystal structure of murine coronin-1: a regulator of actin cytoskeletal dynamics in lymphocytes. *Structure* **14**, 87–96 (2006).
22. McArdle, B. & Hofmann, A. Coronin structure and implications. *Subcell. Biochem.* **48**, 56–71 (2008).
23. Goode, B.L. *et al.* Coronin promotes the rapid assembly and cross-linking of actin filaments and may link the actin and microtubule cytoskeletons in yeast. *J. Cell Biol.* **144**, 83–98 (1999).
24. Galkin, V.E. *et al.* Remodeling of actin filaments by ADF/cofilin proteins. *Proc. Natl. Acad. Sci. USA* **108**, 20568–20572 (2011).
25. Gandhi, M., Jangi, M. & Goode, B.L. Functional surfaces on the actin-binding protein coronin revealed by systematic mutagenesis. *J. Biol. Chem.* **285**, 34899–34908 (2010).
26. Fujii, T., Iwane, A.H., Yanagida, T. & Namba, K. Direct visualization of secondary structures of F-actin by electron cryomicroscopy. *Nature* **467**, 724–728 (2010).
27. Murakami, K. *et al.* Structural basis for actin assembly, activation of ATP hydrolysis, and delayed phosphate release. *Cell* **143**, 275–287 (2010).
28. Fisher, A.J. *et al.* Structural studies of myosin:nucleotide complexes: a revised model for the molecular basis of muscle contraction. *Biophys. J.* **68**, 19S–28S (1995).
29. Fisher, A.J. *et al.* X-ray structures of the myosin motor domain of *Dictyostelium discoideum* complexed with MgADP.BeFx and MgADP.AIF4. *Biochemistry* **34**, 8960–8972 (1995).
30. Combeau, C. & Carlier, M.F. Probing the mechanism of ATP hydrolysis on F-actin using vanadate and the structural analogs of phosphate BeF_3^- and AlF_4. *J. Biol. Chem.* **263**, 17429–17436 (1988).
31. Malm, B., Larsson, H. & Lindberg, U. The profilin–actin complex: further characterization of profilin and studies on the stability of the complex. *J. Muscle Res. Cell Motil.* **4**, 569–588 (1983).
32. Duong, A.M. & Reisler, E. C-terminus on actin: spectroscopic and immunochemical examination of its role in actomyosin interactions. *Adv. Exp. Med. Biol.* **358**, 59–70 (1994).
33. Crosbie, R.H., Chalovich, J.M. & Reisler, E. Interaction of caldesmon and myosin subfragment 1 with the C-terminus of actin. *Biochem. Biophys. Res. Commun.* **184**, 239–245 (1992).
34. Kudryashov, D.S. & Reisler, E. ATP and ADP actin states. *Biopolymers* **99**, 245–256 (2013).
35. Chen, T., Applegate, D. & Reisler, E. Cross-linking of actin to myosin subfragment 1 in the presence of nucleotides. *Biochemistry* **24**, 5620–5625 (1985).
36. Andreev, O.A., Saraswat, L.D., Lowey, S., Slaughter, C. & Borejdo, J. Interaction of the N-terminus of chicken skeletal essential light chain 1 with F-actin. *Biochemistry* **38**, 2480–2485 (1999).
37. Sutoh, K. Identification of myosin-binding sites on the actin sequence. *Biochemistry* **21**, 3654–3661 (1982).
38. Crosbie, R.H., Miller, C., Chalovich, J.M., Rubenstein, P.A. & Reisler, E. Caldesmon, N-terminal yeast actin mutants, and the regulation of actomyosin interactions. *Biochemistry* **33**, 3210–3216 (1994).
39. Grintsevich, E.E. *et al.* Mapping of drebrin binding site on F-actin. *J. Mol. Biol.* **398**, 542–554 (2010).
40. Galkin, V.E. *et al.* Coronin-1A stabilizes F-actin by bridging adjacent actin protomers and stapling opposite strands of the actin filament. *J. Mol. Biol.* **376**, 607–613 (2008).
41. Johara, M. *et al.* Charge-reversion mutagenesis of *Dictyostelium* actin to map the surface recognized by myosin during ATP-driven sliding motion. *Proc. Natl. Acad. Sci. USA* **90**, 2127–2131 (1993).
42. Miller, C.J. & Reisler, E. Role of charged amino acid pairs in subdomain-1 of actin in interactions with myosin. *Biochemistry* **34**, 2694–2700 (1995).
43. Katoh, T. & Morita, F. Mapping myosin-binding sites on actin probed by peptides that inhibit actomyosin interaction. *J. Biochem.* **120**, 580–586 (1996).
44. Grintsevich, E.E. *et al.* Mapping of drebrin binding site on F-actin. *J. Mol. Biol.* **398**, 542–554 (2010).
45. Vancompernolle, K., Vandekerckhove, J., Bubb, M.R. & Korn, E.D. The interfaces of actin and *Acanthamoeba* actobindin: identification of a new actin-binding motif. *J. Biol. Chem.* **266**, 15427–15431 (1991).
46. Ouporov, I.V., Knull, H.R. & Thomasson, K.A. Brownian dynamics simulations of interactions between aldolase and G- or F-actin. *Biophys. J.* **76**, 17–27 (1999).
47. Suarez, C. *et al.* Cofilin tunes the nucleotide state of actin filaments and severs at bare and decorated segment boundaries. *Curr. Biol.* **21**, 862–868 (2011).
48. Rouiller, I. *et al.* The structural basis of actin filament branching by the Arp2/3 complex. *J. Cell Biol.* **180**, 887–895 (2008).
49. Splettstoesser, T., Holmes, K.C., Noe, F. & Smith, J.C. Structural modeling and molecular dynamics simulation of the actin filament. *Proteins* **79**, 2033–2043 (2011).
50. Kudryashov, D.S., Grintsevich, E.E., Rubenstein, P.A. & Reisler, E. A nucleotide state-sensing region on actin. *J. Biol. Chem.* **285**, 25591–25601 (2010).
51. Otterbein, L.R., Graceffa, P. & Dominguez, R. The crystal structure of uncomplexed actin in the ADP state. *Science* **293**, 708–711 (2001).
52. Zheng, X., Diraviyam, K. & Sept, D. Nucleotide effects on the structure and dynamics of actin. *Biophys. J.* **93**, 1277–1283 (2007).
53. Strzelecka-Gołaszewska, H., Mossakowska, M., Wozniak, A., Moraczewska, J. & Nakayama, H. Long-range conformational effects of proteolytic removal of the last three residues of actin. *Biochem. J.* **307**, 527–534 (1995).

ONLINE METHODS

Purification of actin and Crn1ΔCC. Rabbit skeletal-muscle α-actin was prepared according to Spudich and Watt[54] and kept in buffer A (5 mM Tris, pH 8.0, 0.5 mM β-mercaptoethanol, 0.2 mM ATP, and 0.2 mM CaCl₂). Baker's yeast and yeast actin-mutant strains DNEQ[38], ΔDSE[38], R37A R39A[55], K50A D51A[56], D80A D81A[42], E83A D84A[42], E99A E100A[42], K315A E316A[57], and D363A E364A[55] were purified by DNase I affinity chromatography[58]. Yeast actin was cycled after purification as previously described[58] and kept in buffer B (10 mM HEPES, pH 7.4, 1 mM dithiothreitol (DTT), 0.2 mM ATP, and 0.2 mM CaCl₂) on ice. Bacterial expression plasmids for full-length and GST-Crn1ΔCC (residues 1–600) were kindly provided by B. Goode (Brandeis University)[25]. Coronin proteins were expressed in *Escherichia coli* strain BL21 (DE3) and purified as previously described[25].

Preparation of coronin–actin complexes. Rabbit α-actin was dialyzed into buffer C (10 mM Tris, pH 7.5, 0.2 mM CaCl₂, 0.2 mM ATP and 1 mM DTT). The resulting Ca-ATP–actin was exchanged to Mg-ATP–actin (with 50 μM MgCl₂ and 0.4 mM EGTA) over 5 min. Subsequently, 20 μM Mg-ATP–actin was polymerized with 1 mM MgCl₂ and 50 mM KCl for 15 min at room temperature and then kept on ice. ADP–BeFx–actin was prepared by incubation of F-actin with 0.1 mM BeCl₂ and 5 mM NaF for 1–2 h on ice. Coronin was dialyzed into buffer C containing 50 mM KCl. Samples for cryo-EM were prepared by dilution of ADP–BeFx–F-actin to 2 μM in the presence of 6–8 μM Crn1ΔCC (final concentration). ADP–F-actin was prepared from Mg-ATP–actin in buffer C with additional 0.3 mM ATP. After 30 min polymerization at room temperature, 8 units/ml hexokinase and 1 mM dextrose were added to deplete the remaining ATP over 1 h, on ice. Samples for cryo-EM were later prepared by dilution of the stock ADP–F-actin (20 μM) to 2 μM in the presence of 6–8 μM Crn1ΔCC with an F buffer (buffer C with 1 mM MgCl₂, 50 mM KCl and no ATP) supplemented with 0.5 mM ADP.

Cryo-electron microscopy and refinement. An aliquot of sample was applied to Quatifoil 1.2/1.3 grids (with an actual hole size of 1.6 μm). These grids were treated with ethylene dichloride, coated with fresh carbon and baked under a 100-keV electron beam overnight[59]. The grid was then blotted and vitrified in liquid nitrogen–cooled liquid ethane, in a Vitrobot (FEI) machine. The vitrification parameters were: blot force, 1; blot time, 4 s; blot once; wait time, 2 s; drain time, 2s; sample volume applied to each grid, 2.5 μL.

Each grid was loaded into an FEI Titan Krios microscope with autoloader. The microscope was operated at 120 kV. Cryo-EM images were recorded digitally with a Gatan Ultrascan 16-megapixel CCD camera at 59,000× magnification. The calibrated pixel size is 1.437 Å. A total of 1,380 and 1,200 CCD frames were recorded for ADP and ADP–BeFx states, respectively. The defocus values ranged from 2 to 4 μm.

Image quality was then evaluated by Fourier transforms. Decorated actin filaments were selected manually with EMAN helixboxer[60]. A total of 883 and 348 images were used for the final reconstruction for ADP and ADP–BeFx states, respectively. Other images were rejected by evaluation of Fourier spectra. The selected filaments were segmented into boxes by 88% overlap, giving 53,001 and 45,307 boxes (103,800 and 88,080 asymmetric units) for ADP and ADP–BeFx states, respectively. (Each box has dimensions of 320 × 320 pixels, giving about 1 1/4 repeats of actin per box.) We then sorted each data set against our early reconstructions of coronin-decorated actin filaments in ADP and ADP–BeFx states and in undecorated actin filaments. In each data set, we kept the population that aligned best with the model corresponding to the desired state. (The alignments are scored by EMAN with Fourier-ring correlation option.) Among the selected particles, we cut off those with EMAN alignment scores that were one or more s.d. worse than average. The total numbers of boxes used for reconstruction were 31,141 and 26,805 (60,720 and 52,260 asymmetric units) for ADP and ADP–BeFx states, respectively.

We then performed single particle–based helical reconstruction on each set of these particles. We used EMAN–based IHRSR[61] to generate an initial reconstruction for each of the two states. The initial models were generated similarly to previous models[62]. We used a customized version of Relion[63] to do real-space helical reconstructions and finalize the refinement. This 'helical' Relion contains an implementation of IHRSR methods based on Relion's software framework.

We used the gold-standard scheme to estimate our resolutions. The structures were refined with the autorefine function of Relion until convergence.

Modeling of coronin-decorated actin filaments. We built a homology model for yeast coronin 1 based on the crystal structure of mouse coronin 1a (PDB 2AQ5)[21], using SWISS-MODEL on the Expasy server[64]. We docked this model and the pseudoatomic model of actin per subunit (PDB 3MFP)[26] into the two structures by Chimera, using the 'fit into map' function. Both models unambiguously fit the corresponding densities in both structures.

We visualized the interaction between coronin and actin in the two states in Chimera and PyMOL (http://www.pymol.org/). The figures that contain cryo-EM envelopes and pseudoatomic structural models were rendered by Chimera[65].

Fluorescence spectroscopy. Rabbit α-actin was labeled with acrylodan at Cys374 as previously described[56]. DTT-free Ca–G-actin was incubated with a two-fold molar excess of acrylodan for 2.5 h, at 24 °C. The labeling reactions were quenched with 1 mM DTT, and this was followed by the removal of excess acrylodan on a G-50 Sephadex column. ADP–F-actin and ADP–BeFx–F-actin samples were prepared from labeled actin as described above. Fluorescence emission spectra of labeled ADP–F-actin and ADP–BeFx–F-actin in the absence and presence of Crn1ΔCC were recorded between 400 and 650 nm, with the excitation wavelength set at 385 nm, using a Photon Technology International (PTI) spectrofluorometer. **Figure 2e,f** shows representative spectra obtained in experiments yielding identical results (two repeats).

Cosedimentation experiments. Cosedimentation experiments were done as previously reported[25], with minor modifications. Crn1ΔCC (1.0 μm) was incubated with increasing concentrations (0–30 μm) of polymerized wild-type and mutant yeast actins for 15 min and then centrifuged for 25 min at 90,000 r.p.m. in a Beckman TLA100 rotor. Pellets and supernatants were run on SDS-PAGE, and the percentage of coronin bound to actin was calculated by densitometry analysis of the corresponding bands on Coomassie-stained gels with Scion Image. The binding curves were obtained with Systat SigmaPlot for each of the independent repeats (mostly three). Representative binding curves are shown in **Supplementary Figure 3**.

Zero-length cross-linking with EDC/NHS. EDC/NHS (Thermo Scientific–Pierce Biotechnology) cross-linking of F-actin and Crn1ΔCC was done according to a two-step reaction protocol[66] according to the manufacturer's instructions. In short, α-skeletal, WT, and DNEQ actins were exchanged into 5 mM MES, pH 6.0, buffer supplemented with 0.2 mM ATP and 0.2 mM CaCl₂ with G-50 desalting columns. 15-μM aliquots of these actins were polymerized as described above. After F-actins were activated with 15 μM EDC and 15 μM sulfo-NHS (for 15 min at 24 °C), excess reagents were quenched with 0.5 mM BME. Crn1ΔCC and NHS-ester–activated F-actins were mixed to a final concentration of 10 μM each, and the pH of the solution was raised above pH 7.0 (with 1 M HEPES buffer, pH 7.6) to initiate cross-linking reactions. Reaction aliquots were taken at different time intervals and run on SDS-PAGE gels.

54. Spudich, J.A. & Watt, S. The regulation of rabbit skeletal muscle contraction: I. Biochemical studies of the interaction of the tropomyosin-troponin complex with actin and the proteolytic fragments of myosin. *J. Biol. Chem.* **246**, 4866–4871 (1971).
55. Wertman, K.F., Drubin, D.G. & Botstein, D. Systematic mutational analysis of the yeast *ACT1* gene. *Genetics* **132**, 337–350 (1992).
56. Oztug Durer, Z.A., Kamal, J.K., Benchaar, S., Chance, M.R. & Reisler, E. Myosin binding surface on actin probed by hydroxyl radical footprinting and site-directed labels. *J. Mol. Biol.* **414**, 204–216 (2011).
57. Korman, V.L. & Tobacman, L.S. Mutations in actin subdomain 3 that impair thin filament regulation by troponin and tropomyosin. *J. Biol. Chem.* **274**, 22191–22196 (1999).
58. Durer, Z.A. *et al.* Structural states and dynamics of the D-loop in actin. *Biophys. J.* **103**, 930–939 (2012).
59. Ge, P., Poweleit, N., Gunsalus, R.P. & Zhou, Z.H. Deriving *de novo* atomic models by cryo electron microscopy. *J. Vis. Exp.* (in the press).
60. Ludtke, S.J., Baldwin, P.R. & Chiu, W. EMAN: semi-automated software for high resolution single particle reconstructions. *J. Struct. Biol.* **128**, 82–97 (1999).

61. Ge, P. & Zhou, Z.H. Hydrogen-bonding networks and RNA bases revealed by cryo electron microscopy suggest a triggering mechanism for calcium switches. *Proc. Natl. Acad. Sci. USA* **108**, 9637–9642 (2011).
62. Ge, P. *et al.* Cryo-EM model of the bullet-shaped vesicular stomatitis virus. *Science* **327**, 689–693 (2010).
63. Scheres, S.H.W. RELION: implementation of a Bayesian approach to cryo-EM structure determination. *J. Struct. Biol.* **180**, 519–530 (2012).
64. Arnold, K., Bordoli, L., Kopp, J. & Schwede, T. The SWISS-MODEL workspace: a web-based environment for protein structure homology modelling. *Bioinformatics* **22**, 195–201 (2006).
65. Pettersen, E.F. *et al.* UCSF Chimera: a visualization system for exploratory research and analysis. *J. Comput. Chem.* **25**, 1605–1612 (2004).
66. Grabarek, Z. & Gergely, J. Zero-length crosslinking procedure with the use of active esters. *Anal. Biochem.* **185**, 131–135 (1990).